

Supporting Information

“Gear-Driven”-Type Chirality Transfer of Tetraphenylethene-Based Supramolecular Organic Frameworks for Peptides in Water

Chaochao Yan,^a Qingfang Li,^a Wannan Yang,^a Jingyu Han,^a Yawen Li,^a Yunhong
Dong,^a Dake Chu,^b Lin Cheng,^a and Liping Cao^{*,a}

^aCollege of Chemistry and Materials Science, Northwest University, Xi’an 710069, P.
R. China.

^bDepartment of Gastroenterology, the First Affiliated Hospital of Xi’an Jiaotong
University, Xi’an 710061, P. R. China

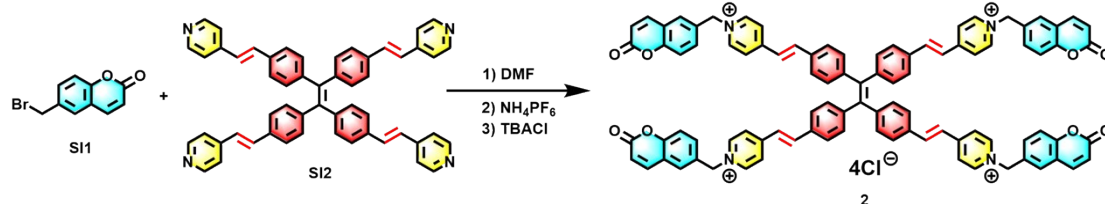
E-mail: chcaoliping@nwu.edu.cn

Table of Contents	Pages
General experimental details	S2
Synthetic procedures and characterization data	S2
NMR, ITC, and Job’s experiments	S9
DLS, UV-vis, and Fluorescence experiments	S11
SEM, TEM, and SAXS experiments	S13
Circular dichroism of SOFs with peptides	S15

Experimental Procedures

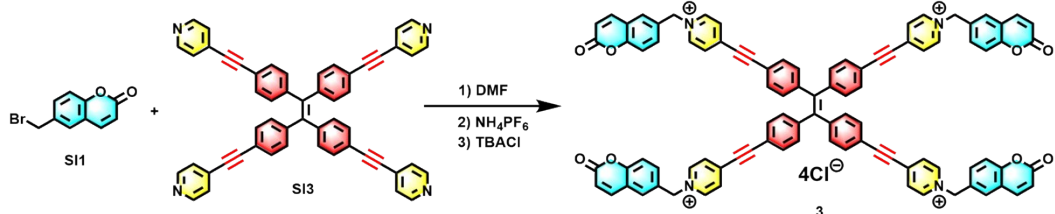
General Experimental Details. Starting materials were purchased from commercial suppliers were used without further purification. Compound **1** was synthesized according to the reported literature.¹ Melting points were recorded by using a XT-4 apparatus in open capillary tubes. IR spectra were measured on a TENSOR27 spectrometer. NMR spectra were recorded on a spectrometer operating at 400 MHz for ¹H and 100 MHz for ¹³C NMR spectra on Bruker ascend spectrometer and JEOL spectrometer. Electrospray Ionization (ESI) mass spectra were acquired with Bruker micrOTOF-Q II electrospray instrument. UV/vis spectra were done on Agilent Cary-100 spectrometer. Fluorescence spectra were performed by using a Horiba Fluorolog-3 spectrometer and QuantaMaster 8000. The absolute photoluminescence quantum efficiency was acquired by using an integrating sphere. Fluorescence decay profiles were recorded on a Flsp920. DLS and Zeta-Potential was measured on a NanoBrook 90 Plus PALS. SEM images were obtained on Hitachi SU8010 microscope. TEM images were obtained on FEI Talos F200X. Small-angle powder diffraction experiment was recorded on BL16B1 at Shanghai Synchrotron Radiation Facility (SSRF). CD spectra were performed by using JASC J-1500.

Synthetic Procedures and Characterization Data



Compound 2. SI1 (154 mg, 644 μmol) and SI2 (60 mg, 80.5 μmol) were added to DMF (4 mL) and the mixture was stirred for another 24 h at 100°C. Then the reaction mixture was cooled, and an excess amount of acetone (200 mL) was added to the solution. The precipitate was filtered and washed with petroleum ether and acetone to give rise to a yellow solid. Then the product with excess amount of NH₄PF₆ in H₂O (3 mL) was dissolved and stirred for 12 h, and the precipitate was collected and washed with an

excess amount of H₂O (3 × 20 mL) to give **2**•4PF₆⁻ as a yellow solid. To the solution of **2**•4PF₆⁻ in MeCN (2 mL) was added excess amount of tetrabutylammonium chloride hydrate (TBACl), and the mixture was stirred for another 12 h. The precipitate was collected and washed with an excess amount of MeCN (3 × 10 mL) to give **2**•4Cl⁻ as a yellow solid (101 mg, 82.3%). M.p. >300°C. IR (KBr, cm⁻¹): 3423s, 2927w, 1724s, 1618s, 1596m, 1515w, 1467w, 1168m, 1134w, 1101w, 977m, 911m, 829m, 801m, 532m. ¹H NMR (400 MHz, DMSO): 9.14 (d, *J* = 6.7, 8H), 8.24 (d, *J* = 6.7, 8H), 8.05 (d, *J* = 9.6, 4H), 7.98 (d, *J* = 16.2, 4H), 7.94 (s, 4H), 7.82 (d, *J* = 8.6, 4H), 7.58 (d, *J* = 8.2, 8H), 7.49 (t, *J* = 16.2, 8H), 7.13 (d, *J* = 8.2, 8H), 6.54 (d, *J* = 9.6, 4H), 5.87 (s, 8H). ¹³C NMR (100 MHz, DMSO): 175.2, 167.9, 167.2, 156.5, 156.2, 155.4, 152.1, 151.4, 143.2, 141.2, 140.2, 139.1, 136.9, 135.7, 130.9, 130.1, 124.4, 122.2, 121.96, 52.4. ESI-TOF-MS: *m/z* 726.2192 ([**2**-2Cl⁻]²⁺, calcd. for [C₉₄H₆₈N₄O₈Cl₂]²⁺, 726.2208); 472.8234 ([**2**-Cl⁻]³⁺, calcd. for [C₉₄H₆₈N₄O₈Cl]³⁺, 472.1580); 345.3749 ([**2**-Cl⁻]⁴⁺, calcd. for [C₉₄H₆₈N₄O₈]⁴⁺, 345.3794).



Compound 3. SI1 (156 mg, 651 μmol) and SI3 (60 mg, 81.4 μmol) were added to DMF (4 mL) and the mixture was stirred for another 24 h at 100°C. Then the reaction mixture was cooled, and an excess amount of acetone (200 mL) was added the solution. The precipitate was filtered and washed with petroleum ether and acetone to give rise to a yellow solid. Then the product with excess amount of NH₄PF₆ in H₂O (3 mL) was dissolved and stirred for 12 h, and the precipitate was collected and washed with an excess amount of H₂O (3 × 20 mL) to give **3**•4PF₆⁻ as a yellow solid. To the solution of **3**•4PF₆⁻ in MeCN (2 mL) was added excess amount of TBACl, and the mixture was stirred for another 12 h. The precipitate was collected and washed with an excess

amount of MeCN (3×10 mL) to give $\mathbf{3} \cdot 4\text{Cl}^-$ as a yellow solid (107 mg, 86.8%). M.p. $>300^\circ\text{C}$. IR (KBr, cm^{-1}): 3425s, 3033m, 2216s, 1728s, 1631s, 1573m, 1517w, 1460w, 1388w, 1168m, 1134w, 1101w, 912w, 831m, 784w, 532m. ^1H NMR (400 MHz, DMSO): 9.23 (d, $J = 6.2$, 8H), 8.24 (d, $J = 6.2$, 8H), 8.05 (d, $J = 9.6$, 4H), 7.91 (s, 4H), 7.81 (d, $J = 8.2$, 4H), 7.56 (d, $J = 7.9$, 8H), 7.51 (d, $J = 8.5$, 4H), 7.17 (d, $J = 7.8$, 8H), 6.56 (d, $J = 9.6$, 4H), 5.92 (s, 8H). ^{13}C NMR (100 MHz, DMSO): 160.2, 154.4, 145.5, 145.1, 144.3, 139.5, 133.1, 132.9, 132.1, 130.9, 130.2, 129.8, 119.6, 119.3, 117.8, 117.6, 102.8, 86.8, 62.5. ESI-TOF-MS: m/z 722.1828 ($[\mathbf{3}-2\text{Cl}^-]^{2+}$, calcd. for $[\text{C}_{94}\text{H}_{60}\text{N}_4\text{O}_8\text{Cl}_2]^{2+}$, 722.1895); 469.4687 ($[\mathbf{3}-\text{Cl}^-]^{3+}$, calcd. for $[\text{C}_{94}\text{H}_{60}\text{N}_4\text{O}_8\text{Cl}]^{3+}$, 469.4705); 343.3573 ($[\mathbf{3}-\text{Cl}^-]^{4+}$, calcd. for $[\text{C}_{94}\text{H}_{60}\text{N}_4\text{O}_8]^{4+}$, 343.3628).

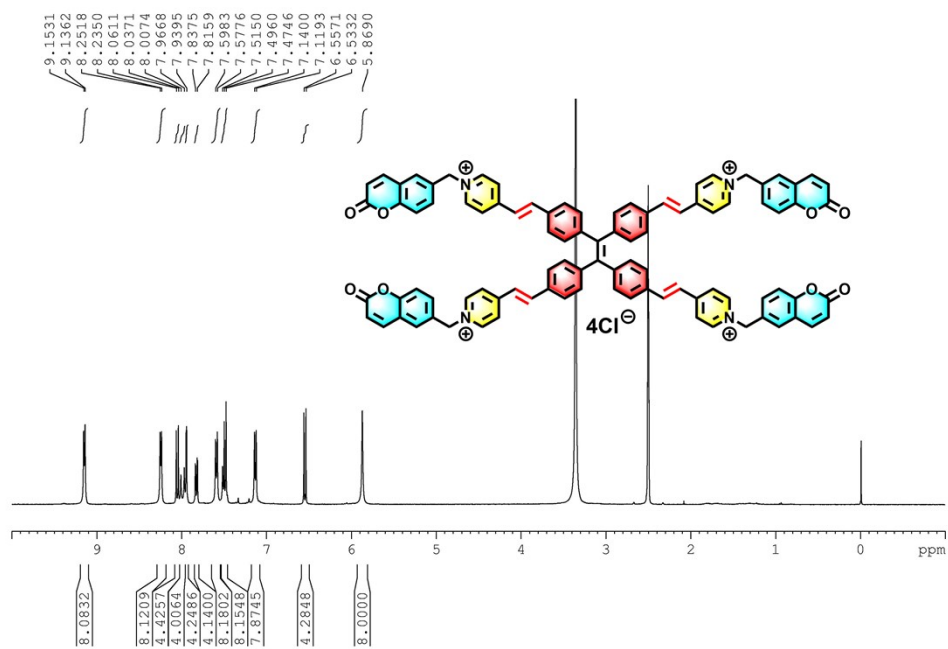


Figure S1. ^1H NMR spectrum recorded (400 MHz, $\text{DMSO-}d_6$, 298 K) for **2**.

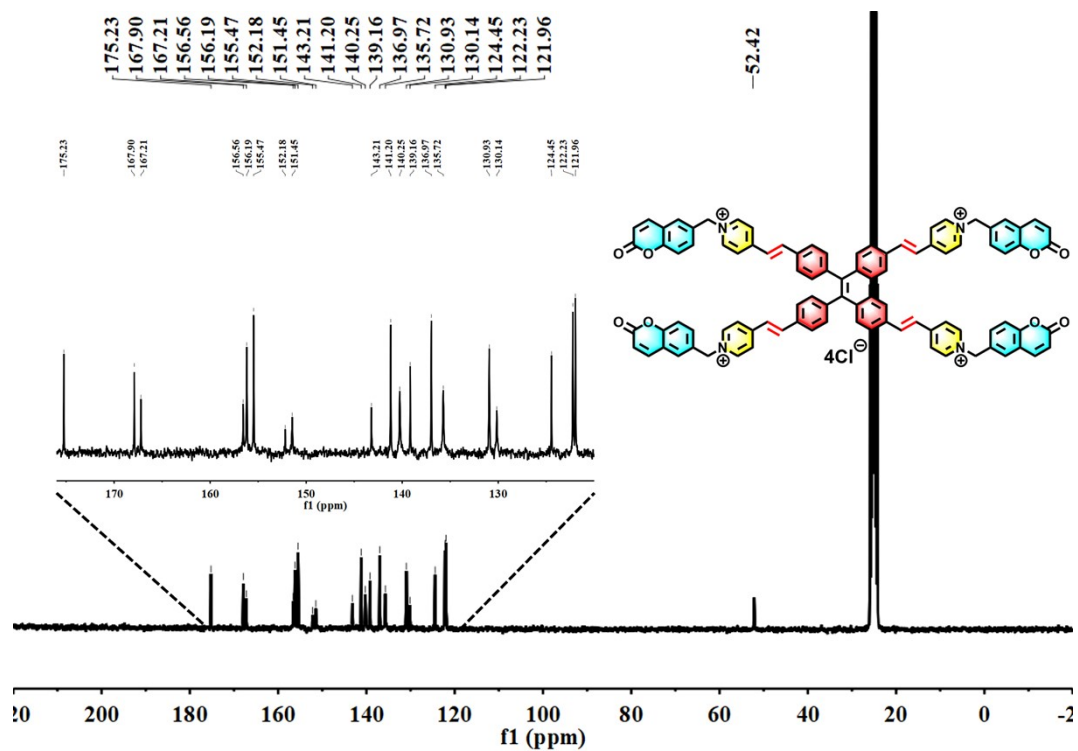


Figure S2. ^{13}C NMR spectrum recorded (100 MHz, $\text{DMSO-}d_6$, 298 K) for **2**.

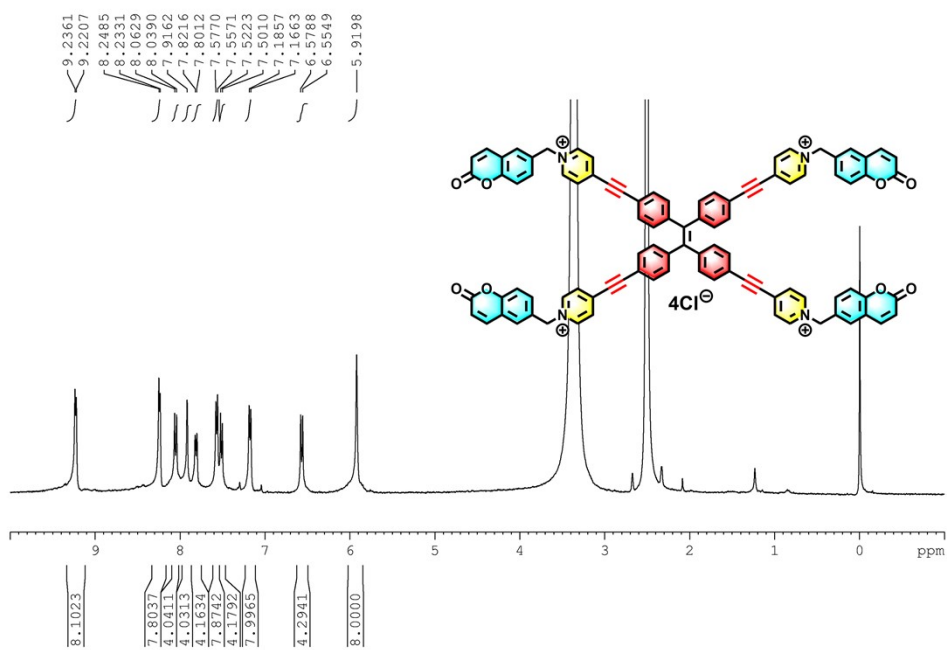


Figure S3. ^1H NMR spectrum recorded (400 MHz, $\text{DMSO-}d_6$, 298 K) for **3**.

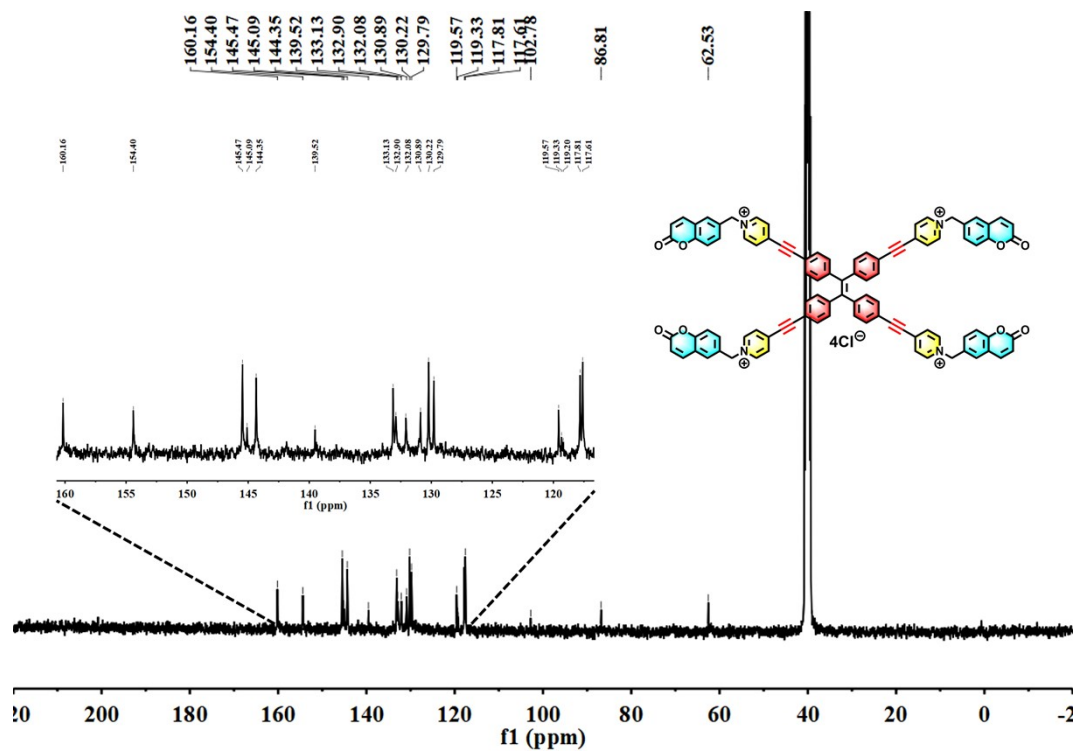


Figure S4. ^{13}C NMR spectrum recorded (100 MHz, $\text{DMSO-}d_6$, 298 K) for **3**.

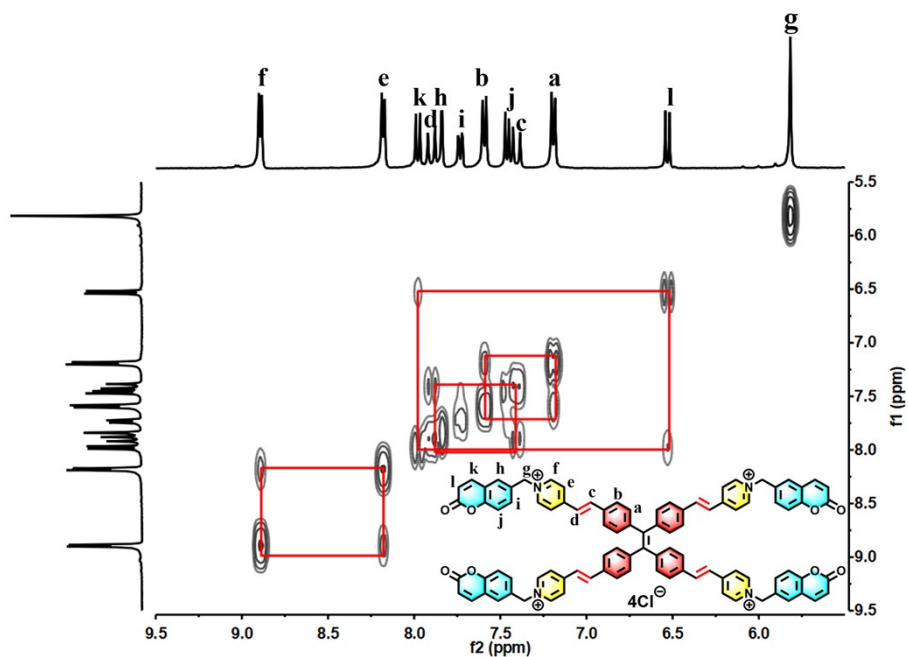


Figure S5. COSY ^1H NMR spectrum recorded (400 MHz, CD_3OD , 298 K) for **2**.

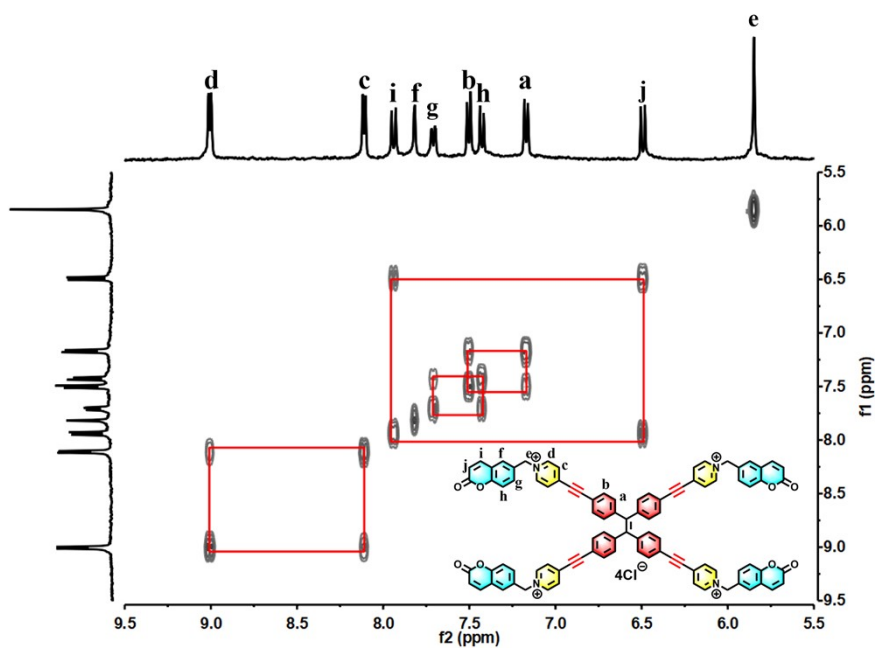


Figure S6. COSY ^1H NMR spectrum recorded (400 MHz, CD_3OD , 298 K) for **3**.

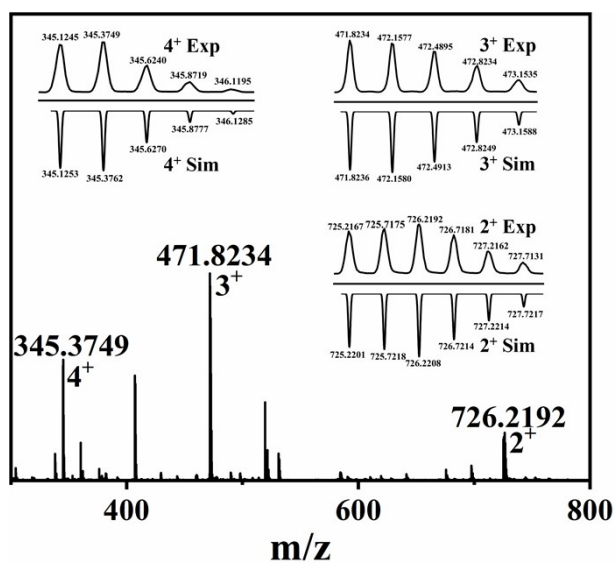


Figure S7. Experimental and calculated electrospray ionization mass spectra of 2.

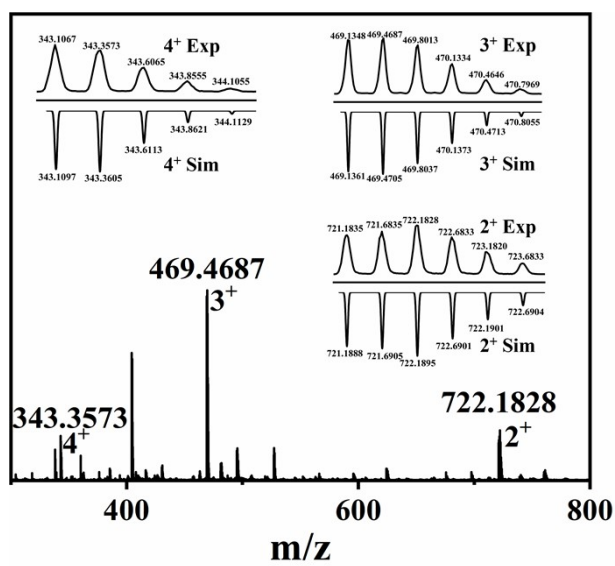


Figure S8. Experimental and calculated electrospray ionization mass spectra of 3.

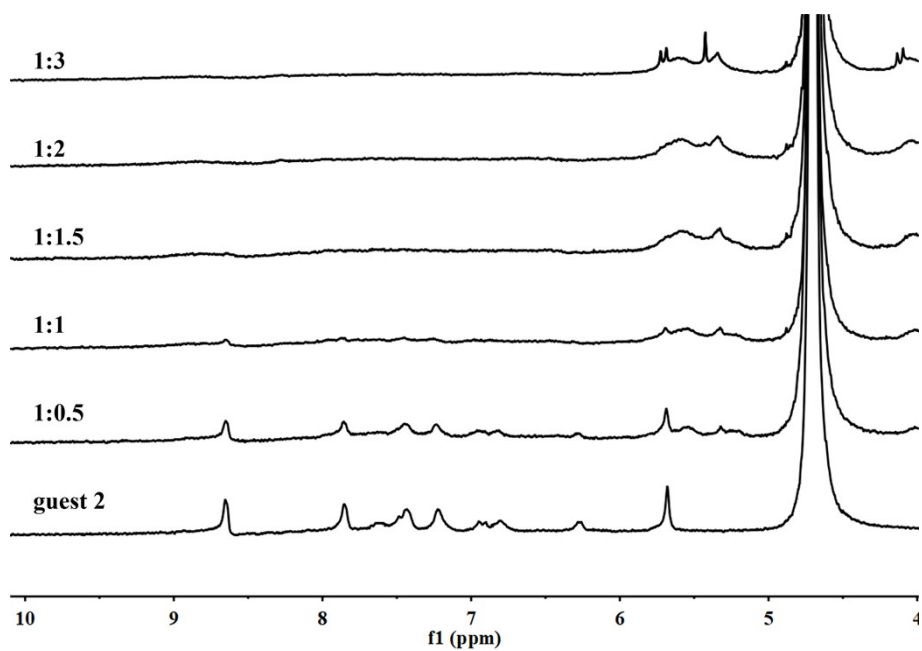


Figure S9. Partial ¹H NMR spectra (400 MHz, 298 K, D₂O) for **2** (0.50 mM) in the presence of CB[8] (0 – 3.0 equiv).

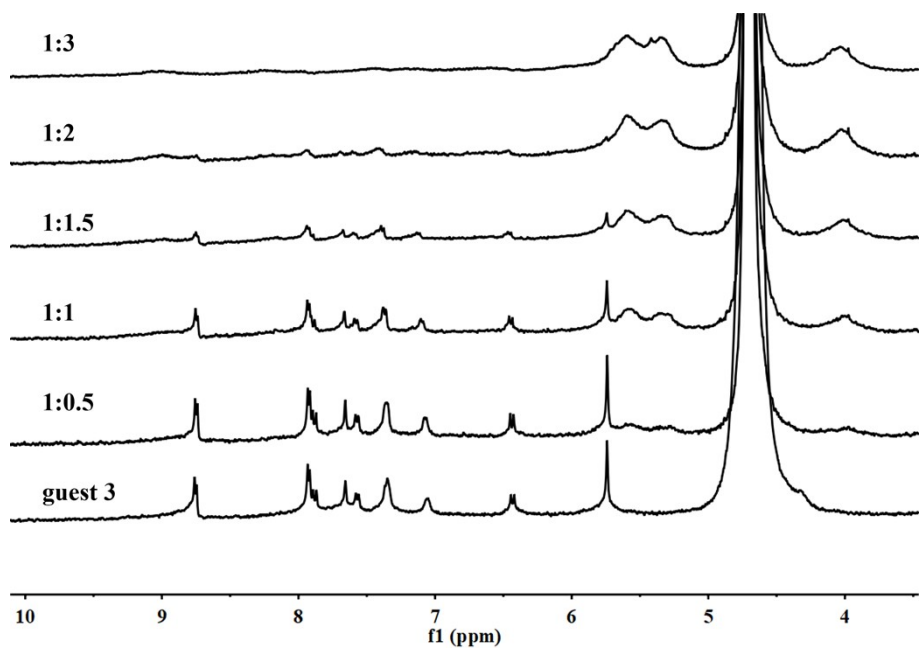


Figure S10. Partial ¹H NMR spectra (400 MHz, 298 K, D₂O) for **3** (0.50 mM) in the presence of CB[8] (0 – 3.0 equiv).

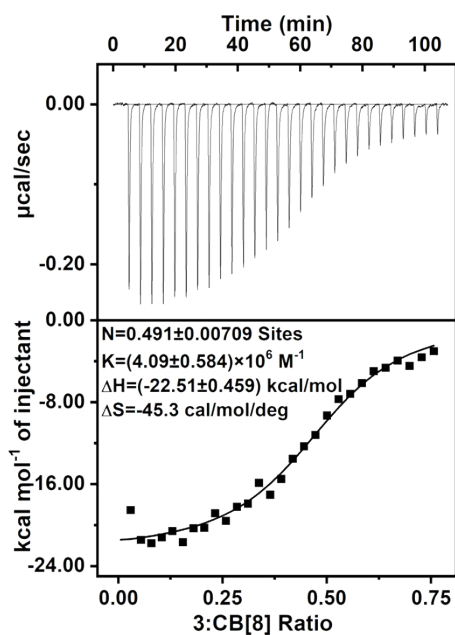


Figure S11. ITC data for the titration of CB[8] (10 μM) in the cell with a solution of **3** in the syringe in H_2O at 298K.

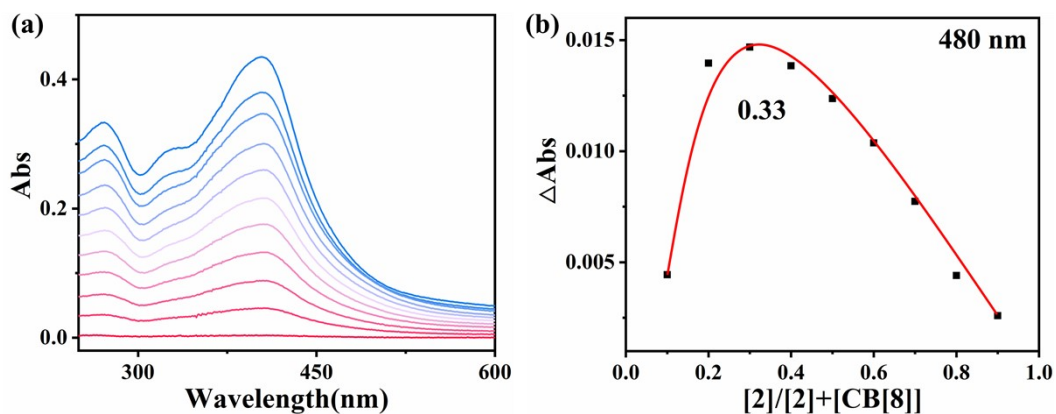


Figure S12. (a) UV-vis spectra and (b) Job's plot obtained by recording the absorption at 480 nm for the solution of **2** and CB[8] ($[\mathbf{2}] + [\text{CB}[8]] = 10 \mu\text{M}$) in water at RT, confirming the 1:2 stoichiometry of their complex.

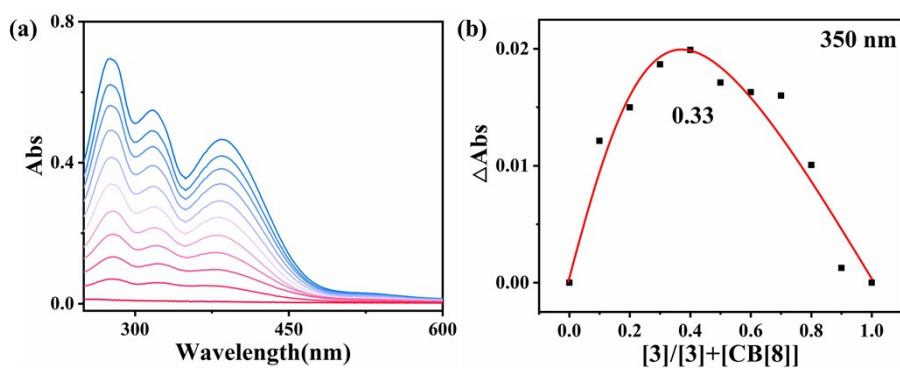


Figure S13. (a) UV-vis spectra and (b) Job's plot obtained by recording the absorption at 480 nm for the solution of **3** and CB[8] ($[3] + [CB[8]] = 10 \mu\text{M}$) in water at RT, confirming the 1:2 stoichiometry of their complex.

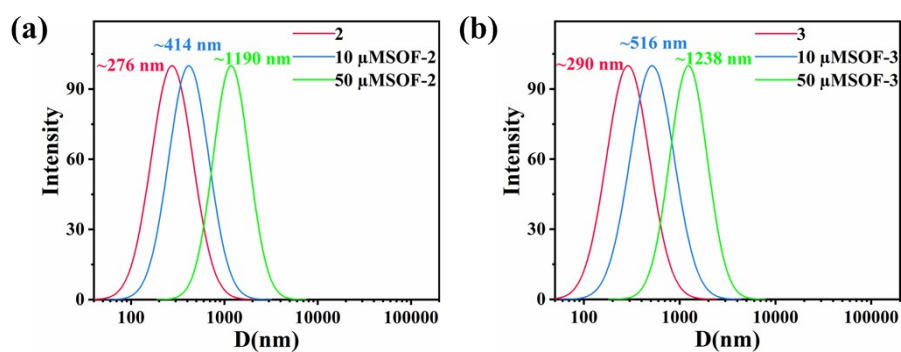


Figure S14. DLS profiles of (a) **2** and **SOF-2**; (b) **3** and **SOF-3** in different concentration.

Table S1. DLS and Zeta-Potential of **2**, **3**, **SOF-2**, and **SOF-3** ($[2] = 10 \mu\text{M}$, $[3] = 10 \mu\text{M}$, and $[CB[8]] = 20 \mu\text{M}$).

Compound	D_h (nm)	Zeta (mV)
2	276.3 ± 1.5	17.9 ± 0.5
SOF-2	413.7 ± 2.9	43.7 ± 0.6
3	290.1 ± 1.1	16.3 ± 1.2
SOF-3	516.5 ± 2.2	39.8 ± 0.6

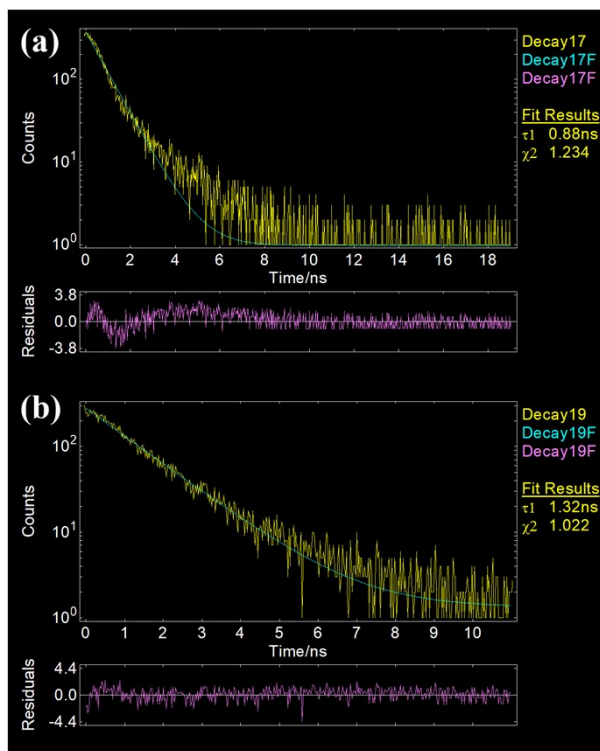


Figure S15. Fluorescence decay profiles of (a) **2** and (b) **SOF-2** in water.

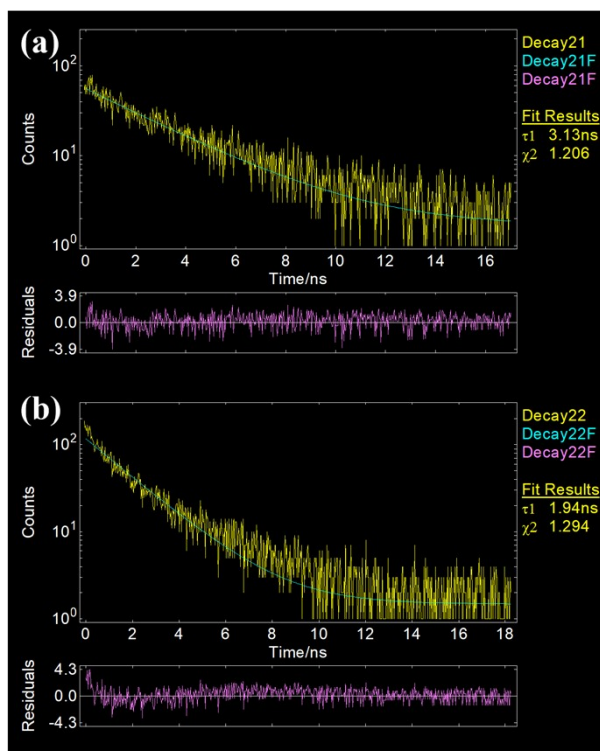


Figure S16. Fluorescence decay profiles of (a) **3** and (b) **SOF-3** in water.

Table S2. Photophysical parameters of **2**, **SOF-2**, **3** and **SOF-3** in water.

Compound	τ (ns) ^a	Φ_F (%) ^b
2	0.88	0.77
SOF-2	1.32	3.31
3	3.13	— ^c
SOF-3	1.94	0.27

^aaverage lifetimes; ^babsolute quantum yield; ^cunmeasurable quantity.

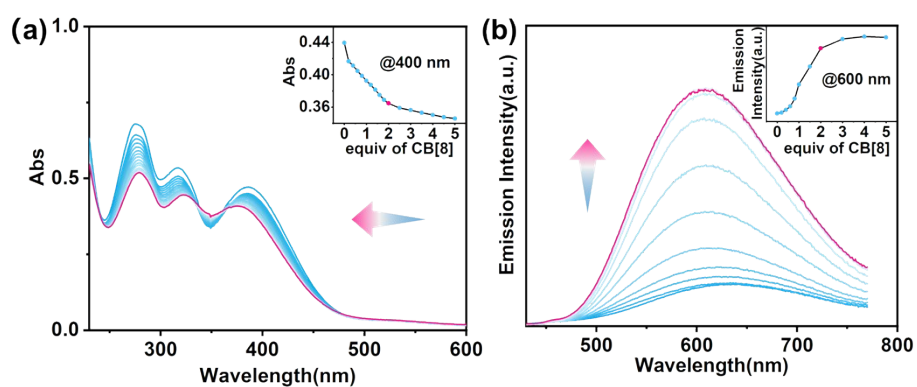


Figure S17. (a) UV-vis absorption and (b) fluorescence spectra of **3** (10 μM) in water upon addition of CB[8] ($\lambda_{\text{ex}} = 395 \text{ nm}$), respectively.

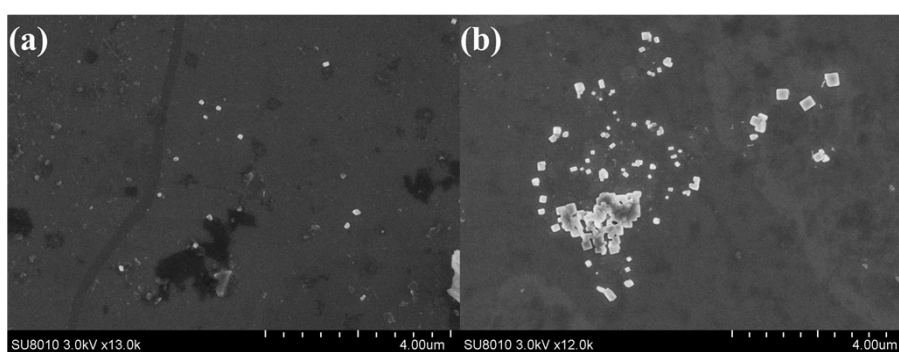


Figure S18. SEM images of the samples from (a) **2** and (b) **SOF-2**. ($[\mathbf{2}] = 10 \mu\text{M}$; $[\text{CB}[8]] = 20 \mu\text{M}$).

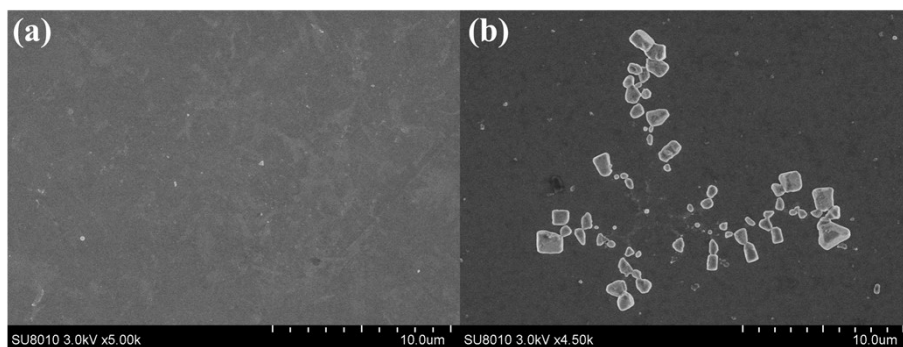


Figure S19. SEM images of the samples from (a) **3** and (b) **SOF-3**. ($[3] = 10 \mu\text{M}$; $[\text{CB}[8]] = 20 \mu\text{M}$).

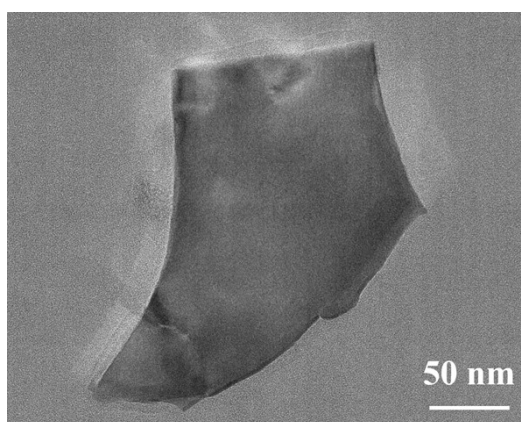


Figure S20. TEM image of the sample from **SOF-3** ($[3] = 50 \mu\text{M}$; $[\text{CB}[8]] = 100 \mu\text{M}$).

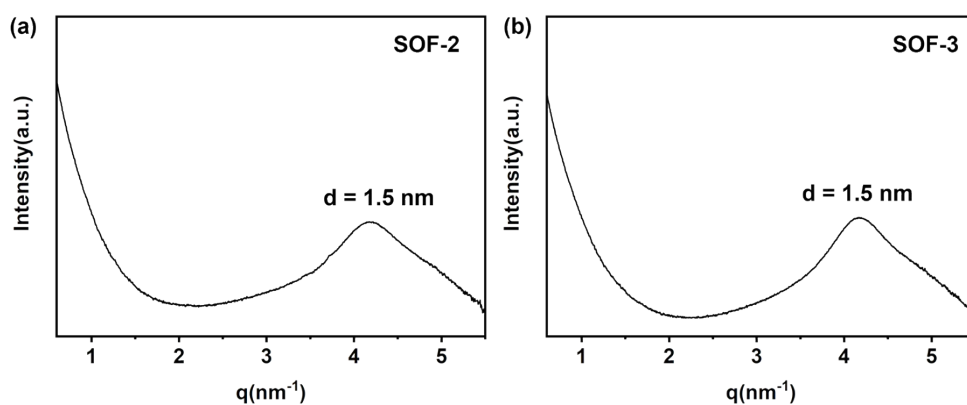


Figure S21. Small-angle synchrotron X-ray-scattering patterns of (a) **SOF-2** and (b) **SOF-3**.

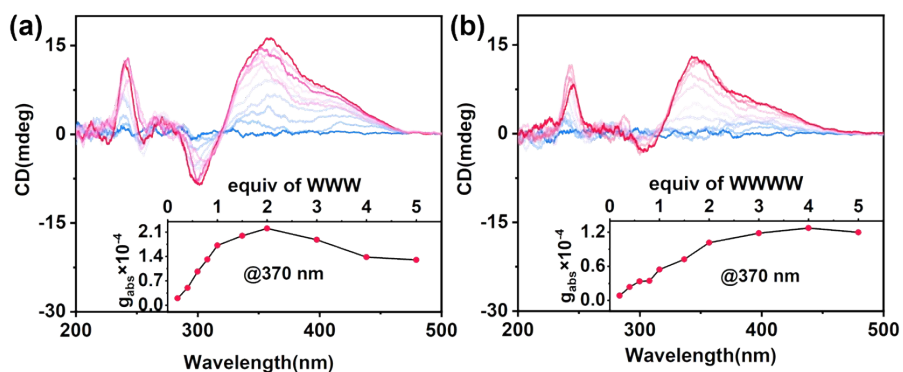


Figure S22. CD spectra of **SOF-1** ($[1] = 50 \mu\text{M}$, $[\text{CB}[8]] = 100 \mu\text{M}$) with (a) WWWW (0 – 0.50 mM) and (b) WWWW (0 – 0.50 mM) in H_2O . Inset: Plots of g_{abs} versus the equiv of guests.

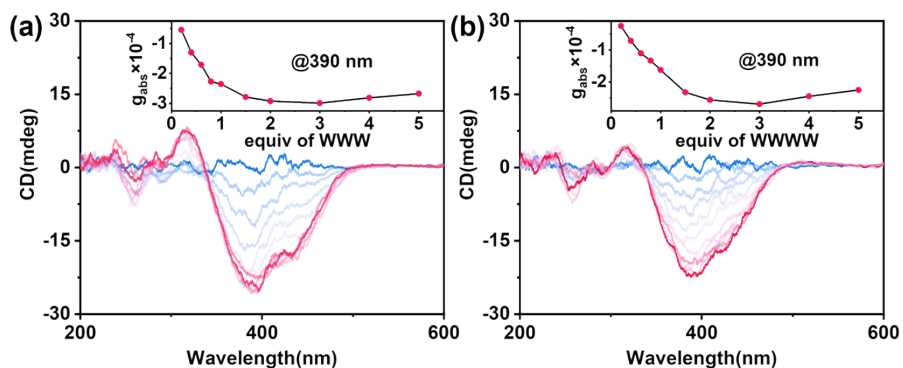


Figure S23. CD spectra of **SOF-2** ($[2] = 50 \mu\text{M}$, $[\text{CB}[8]] = 100 \mu\text{M}$) with (a) WWWW (0 – 0.50 mM) and (b) WWWW (0 – 0.50 mM) in H_2O . Inset: Plots of g_{abs} versus the equiv of guests.

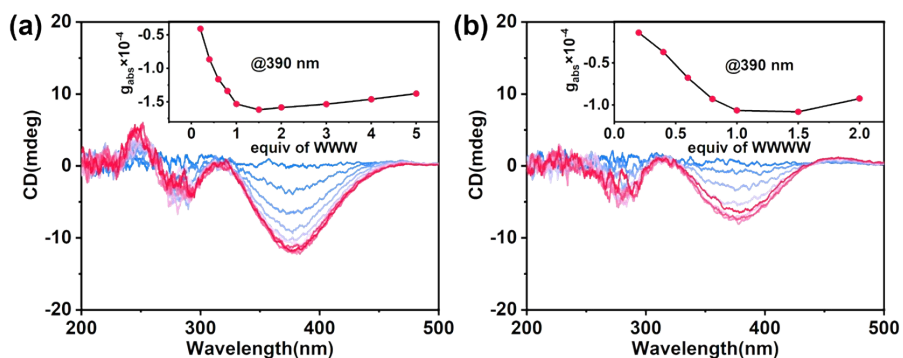


Figure S24. CD spectra of **SOF-3** ($[3] = 50 \mu\text{M}$, $[\text{CB}[8]] = 100 \mu\text{M}$) with (a) WWWW (0 – 0.50 mM) and (b) WWWW (0 – 0.2 mM) in H_2O . Inset: Plots of g_{abs} versus the equiv of guests.

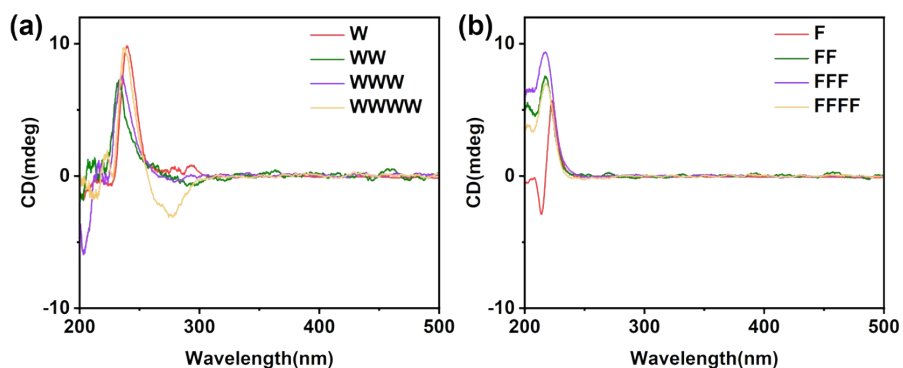


Figure S25. CD spectra recorded of guests in water: (a) W, WW, WWW, WWWW and (b) F, FF, FFF, FFFF.

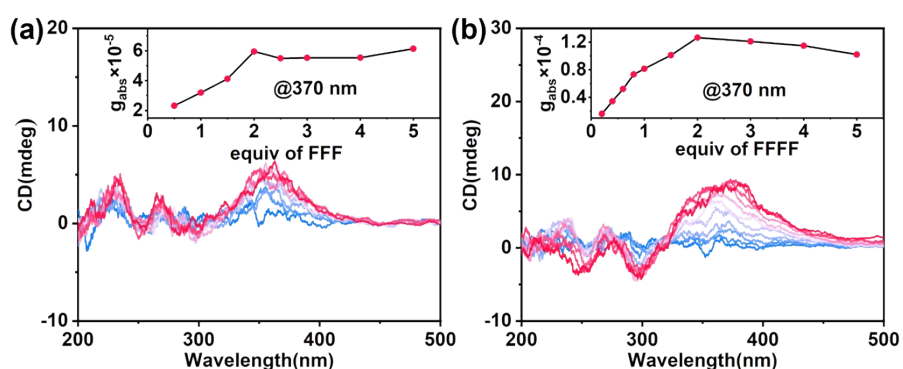


Figure S26. CD spectra of SOF-1 ($[1] = 50 \mu\text{M}$, $[\text{CB}[8]] = 100 \mu\text{M}$) with (a) FFF (0 – 0.50 mM) and (b) FFFF (0 – 0.50 mM) in H_2O . Inset: Plots of g_{abs} versus the equiv of guests.

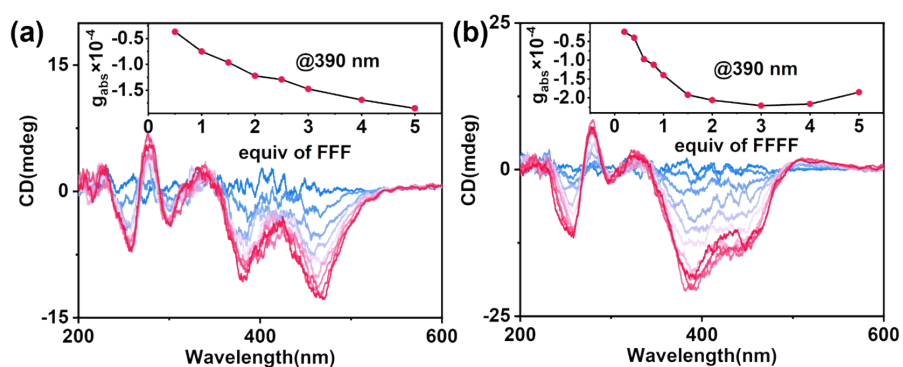


Figure S27. CD spectra of SOF-2 ($[2] = 50 \mu\text{M}$, $[\text{CB}[8]] = 100 \mu\text{M}$) with (a) FFF (0 – 0.50 mM) and (b) FFFF (0 – 0.50 mM) in H_2O . Inset: Plots of g_{abs} versus the equiv of guests.

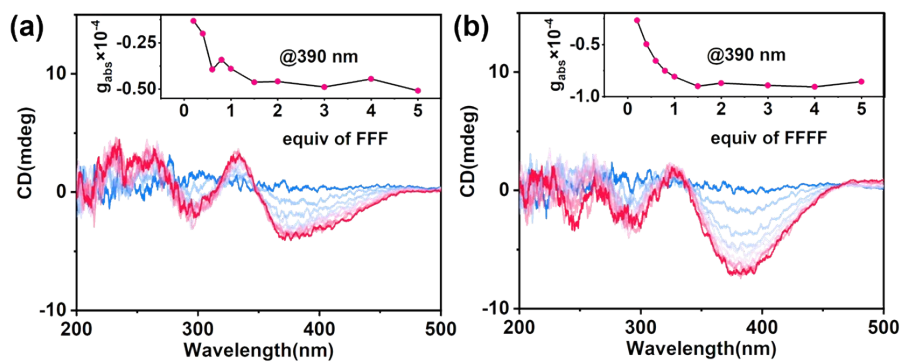


Figure S28. CD spectra of SOF-3 ($[3] = 50 \mu\text{M}$, $[\text{CB}[8]] = 100 \mu\text{M}$) with (a) FFF (0 – 0.50 mM) and (b) FFFF (0 – 0.50 mM) in H₂O. Inset: Plots of g_{abs} versus the equiv of guests.

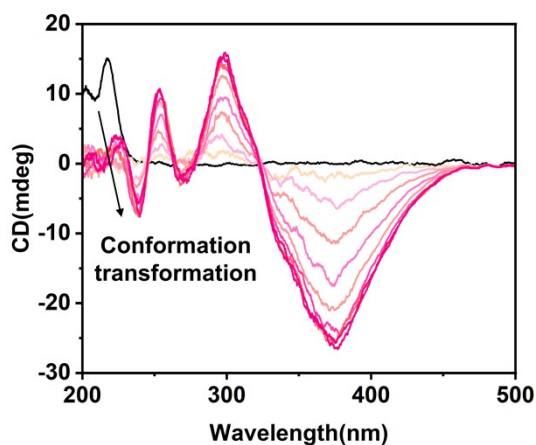


Figure S29. CD spectra on FF alone and SOF-1 with FF (0 – 0.50 mM) in H₂O.

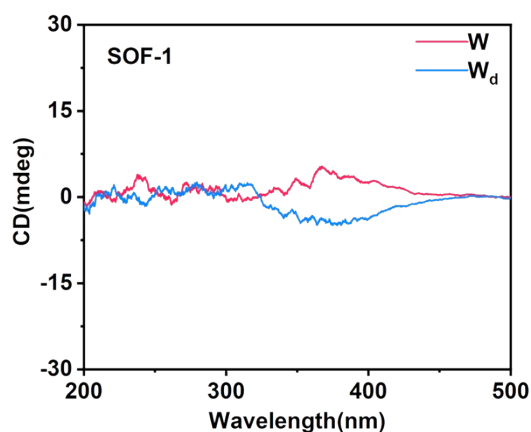


Figure S30. CD spectra of SOF-1 ($[1] = 50 \mu\text{M}$, $[\text{CB}[8]] = 100 \mu\text{M}$) with W (1.50 mM) and W_d (1.50 mM) in H₂O.

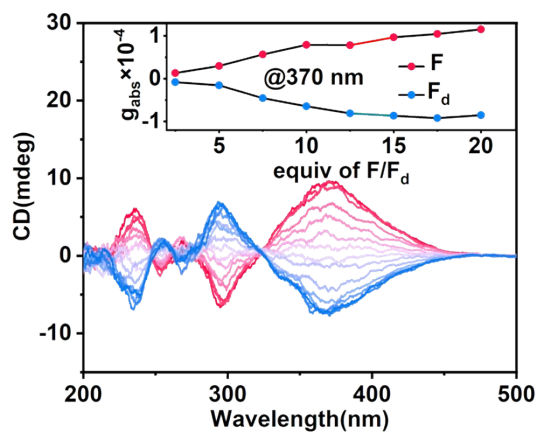


Figure S31. CD spectra of SOF-1 ($[1] = 50 \mu\text{M}$, $[\text{CB}[8]] = 100 \mu\text{M}$) with F (0 – 2.0 mM) and F_d (0 – 2.0 mM) in H_2O . Inset: Plots of g_{abs} versus the equiv of guests.

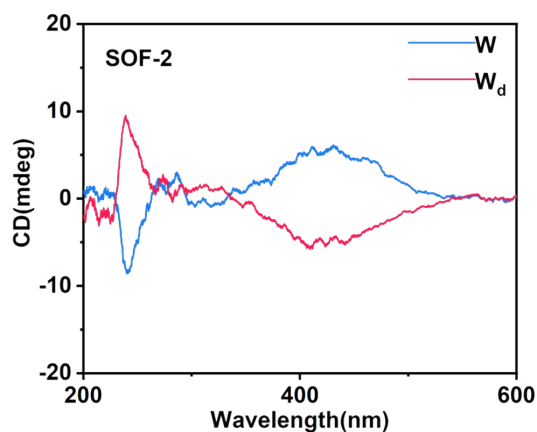


Figure S32. CD spectra of SOF-2 ($[2] = 50 \mu\text{M}$, $[\text{CB}[8]] = 100 \mu\text{M}$) with W (1.50 mM) and W_d (1.50 mM) in H_2O .

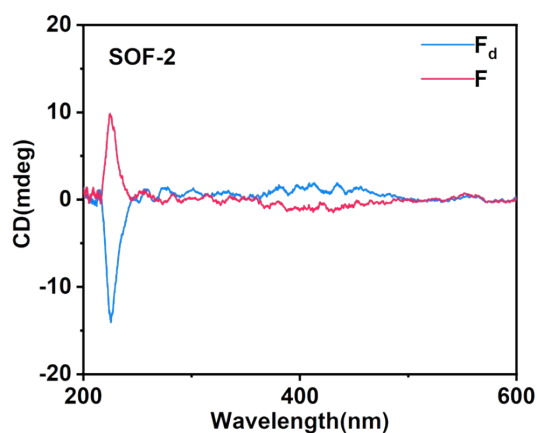


Figure S33. CD spectra of SOF-2 ($[2] = 50 \mu\text{M}$, $[\text{CB}[8]] = 100 \mu\text{M}$) with F (1.50 mM) and F_d (1.50 mM) in H_2O .

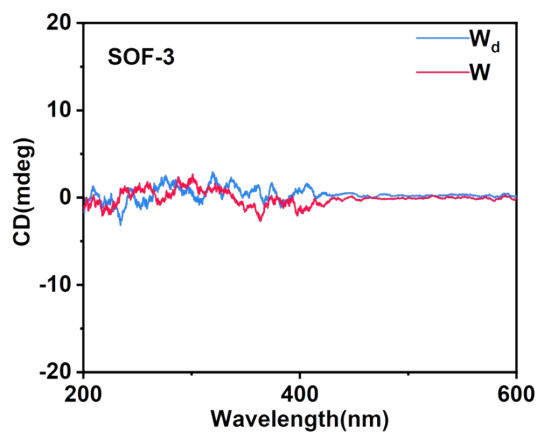


Figure S34. CD spectra of SOF-3 ($[3] = 50 \mu\text{M}$, $[\text{CB}[8]] = 100 \mu\text{M}$) with W (1.50 mM) and W_d (1.50 mM) in H_2O .

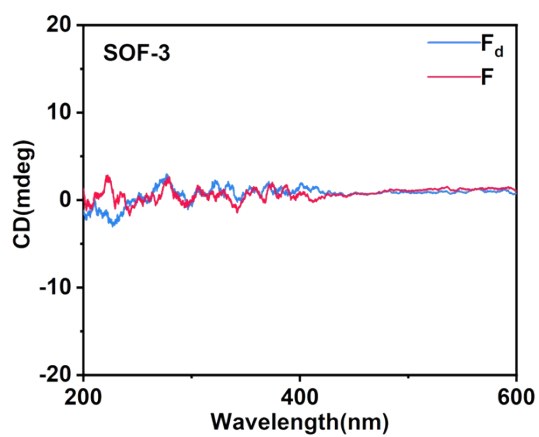


Figure S35. CD spectra of SOF-3 ($[3] = 50 \mu\text{M}$, $[\text{CB}[8]] = 100 \mu\text{M}$) with F (1.50 mM) and F_d (1.50 mM) in H_2O .

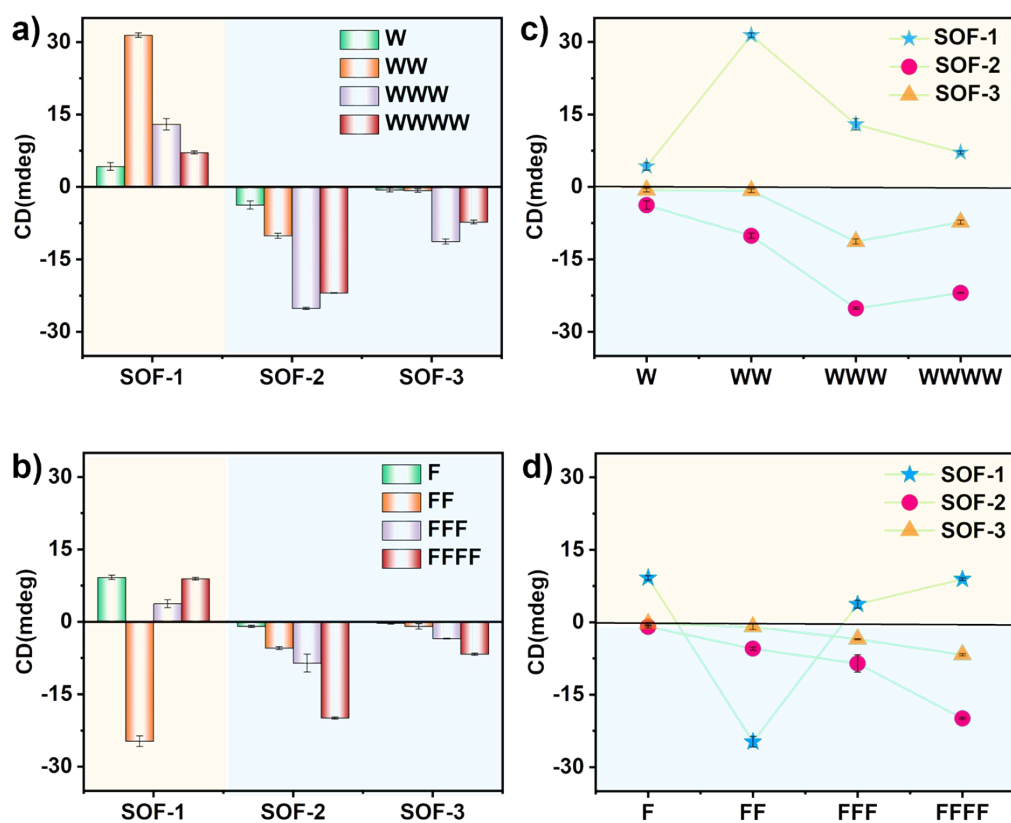


Figure S36. Histograms (a, b) and line plots (c, d) of the CD intensities of SOF-1, SOF-2, and SOF-3 with W-type and F-type chiral guests.

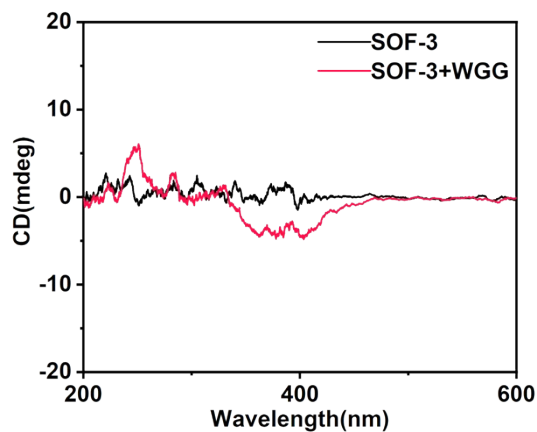


Figure S37. CD spectra of SOF-3 ([3] = 50 μ M, [CB[8]] = 100 μ M) with WGG (1.50 mM) in H₂O.

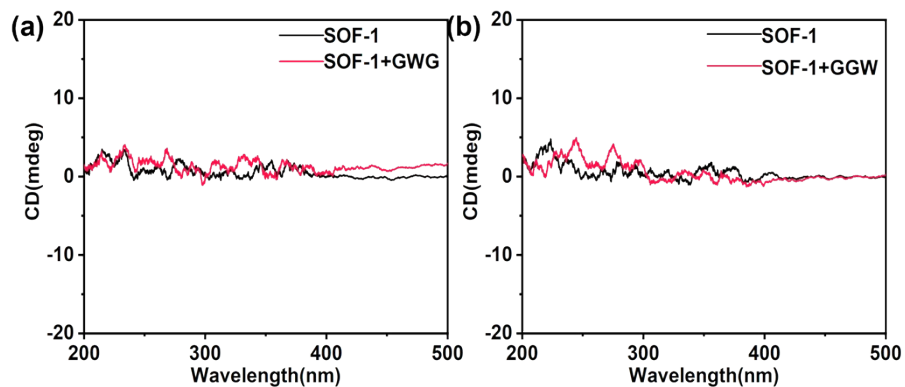


Figure S38. CD spectra of SOF-1 ($[1] = 50 \mu\text{M}$, $[\text{CB}[8]] = 100 \mu\text{M}$) with GWG (1.50 mM) and GGW (1.50 mM) in H_2O .

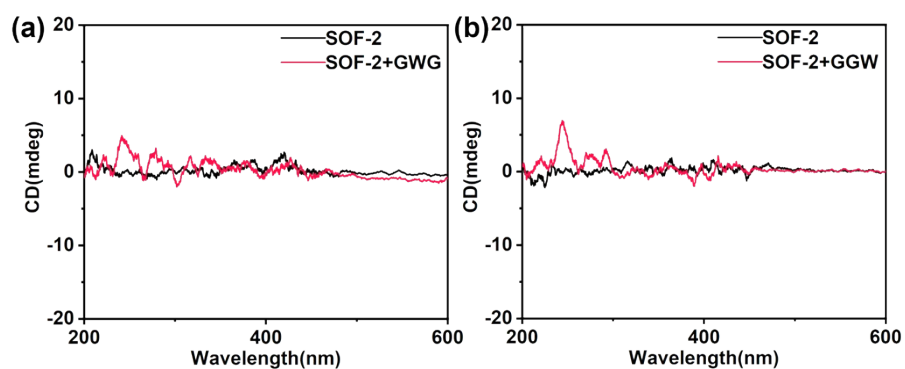


Figure S39. CD spectra of SOF-2 ($[2] = 50 \mu\text{M}$, $[\text{CB}[8]] = 100 \mu\text{M}$) with GWG (1.50 mM) and GGW (1.50 mM) in H_2O .

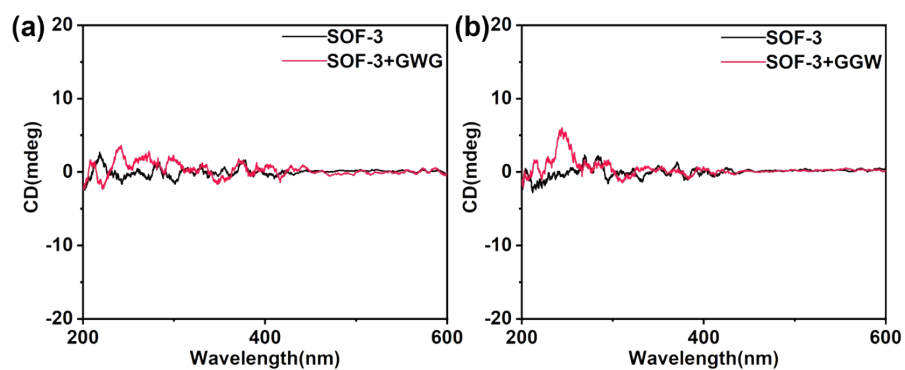


Figure S40. CD spectra of SOF-3 ($[3] = 50 \mu\text{M}$, $[\text{CB}[8]] = 100 \mu\text{M}$) with GWG (1.50 mM) and GGW (1.50 mM) in H_2O .

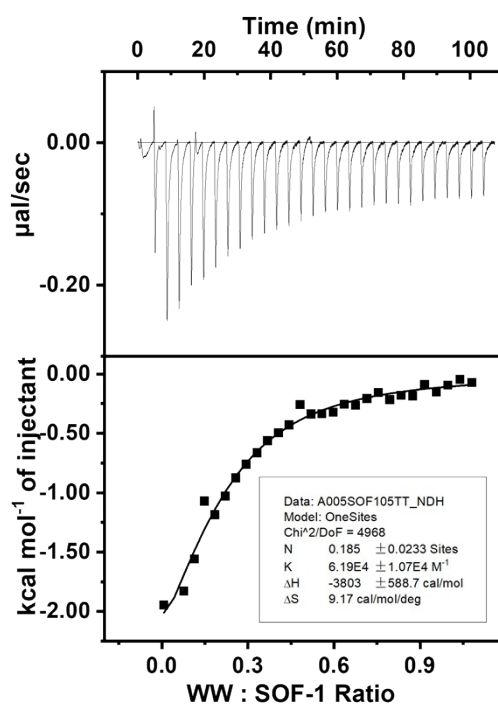


Figure S41. ITC data for the titration of SOF-1 ($[1] = 50 \mu\text{M}$, $[\text{CB}[8]] = 100 \mu\text{M}$) in the cell with a solution of WW (0.5 mM) in the syringe in H_2O at 298K.

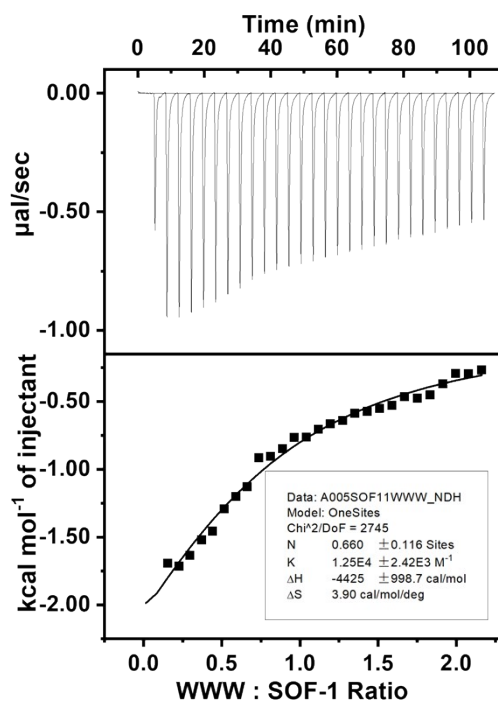


Figure S42. ITC data for the titration of SOF-1 ($[1] = 50 \mu\text{M}$, $[\text{CB}[8]] = 100 \mu\text{M}$) in the cell with a solution of WWW (1.0 mM) in the syringe in H_2O at 298K.

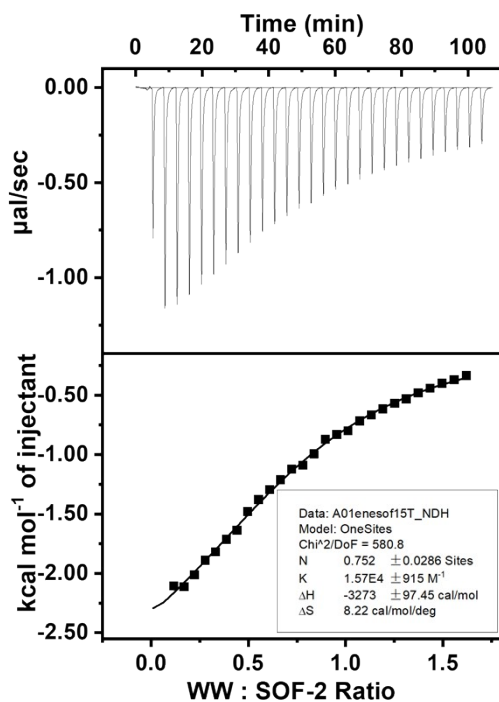


Figure S43. ITC data for the titration of SOF-2 ($[2] = 50 \mu\text{M}$, $[\text{CB}[8]] = 100 \mu\text{M}$) in the cell with a solution of WW (1.5 mM) in the syringe in H_2O at 298K.

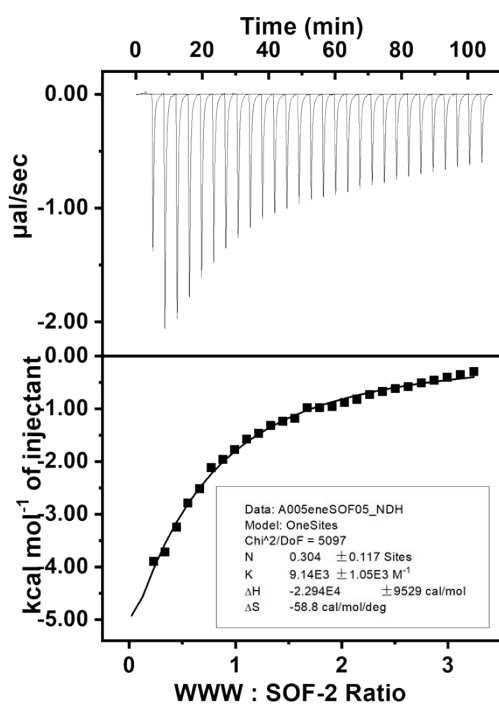


Figure S44. ITC data for the titration of SOF-2 ($[2] = 50 \mu\text{M}$, $[\text{CB}[8]] = 100 \mu\text{M}$) in the cell with a solution of WWW (1.5 mM) in the syringe in H_2O at 298K.

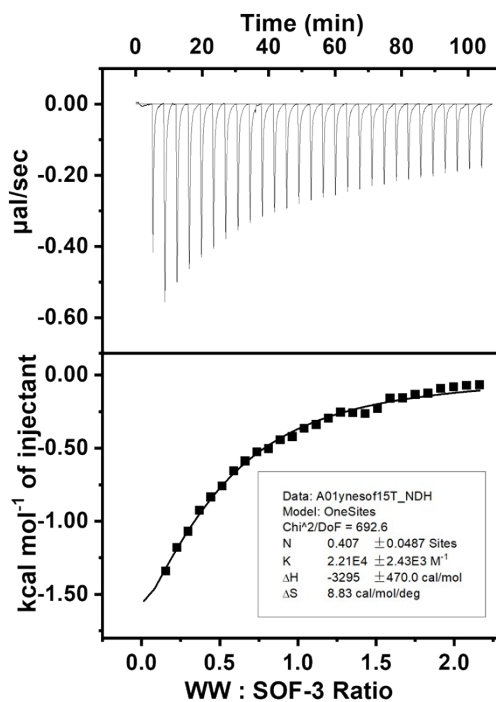


Figure S45. ITC data for the titration of SOF-3 ($[3] = 50 \mu\text{M}$, $[\text{CB}[8]] = 100 \mu\text{M}$) in the cell with a solution of WW (1.5 mM) in the syringe in H_2O at 298K.

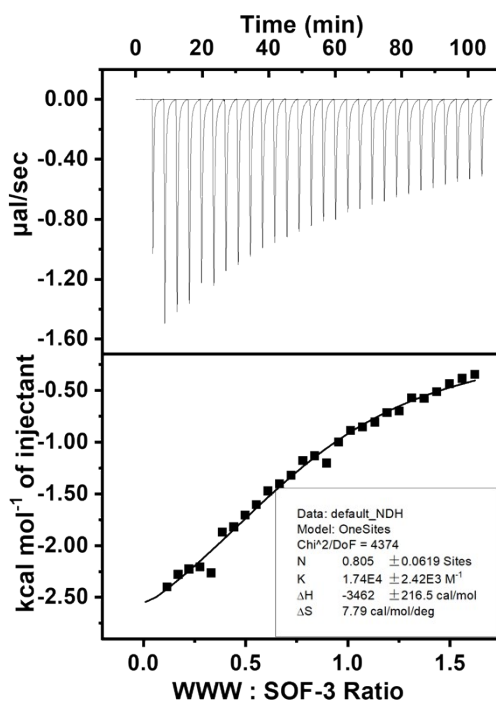


Figure S46. ITC data for the titration of SOF-3 ($[3] = 50 \mu\text{M}$, $[\text{CB}[8]] = 100 \mu\text{M}$) in the cell with a solution of WWW (1.5 mM) in the syringe in H_2O at 298K.

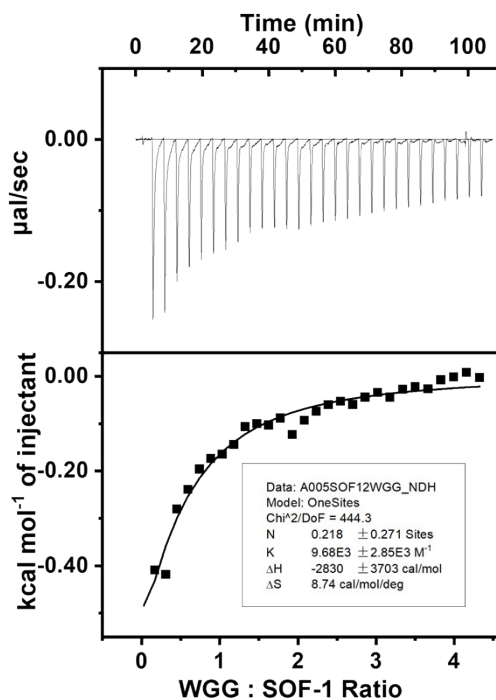


Figure S47. ITC data for the titration of SOF-1 ($[1] = 50 \mu\text{M}$, $[\text{CB}[8]] = 100 \mu\text{M}$) in the cell with a solution of WGG (2 mM) in the syringe in H_2O at 298K.

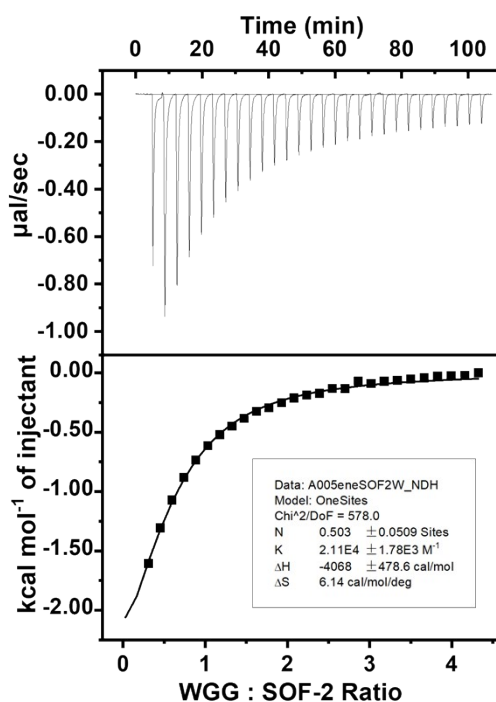


Figure S48. ITC data for the titration of SOF-2 ($[2] = 50 \mu\text{M}$, $[\text{CB}[8]] = 100 \mu\text{M}$) in the cell with a solution of WGG (2 mM) in the syringe in H_2O at 298K.

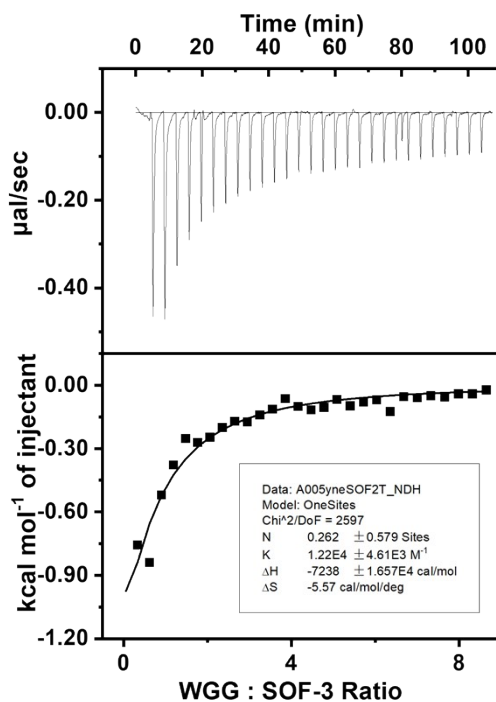


Figure S49. ITC data for the titration of **SOF-3** ($[3] = 50 \mu\text{M}$, $[\text{CB}[8]] = 100 \mu\text{M}$) in the cell with a solution of **WGG** (2 mM) in the syringe in H_2O at 298K .

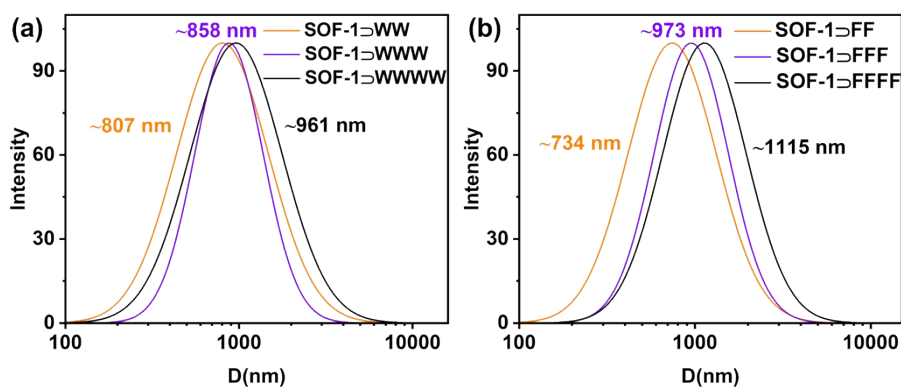


Figure S50. DLS profiles of (a) **SOF-1** Δ **WW** (orange), **SOF-1** Δ **WWW** (purple), **SOF-1** Δ **WWWW** (black), and (b) **SOF-1** Δ **FF** (orange), **SOF-1** Δ **FFF** (purple), **SOF-1** Δ **FFFF** (black) in water ($[1] = 10 \mu\text{M}$, $[\text{CB}[8]] = 20 \mu\text{M}$, and peptides ($20 \mu\text{M}$)).

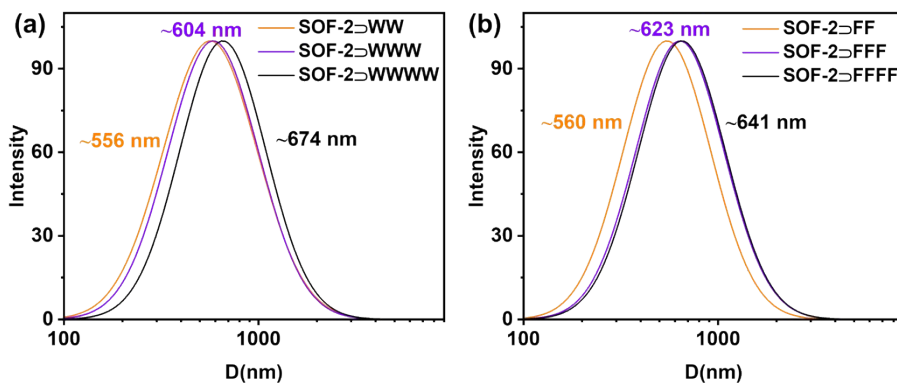


Figure S51. DLS profiles of (a) SOF-2 Δ WW (orange), SOF-2 Δ WWW (purple), SOF-2 Δ WWWW (black), and (b) SOF-2 Δ FF (orange), SOF-2 Δ FFF (purple), SOF-2 Δ FFFF (black) in water ($[2] = 10 \mu\text{M}$, $[\text{CB}[8]] = 20 \mu\text{M}$, and peptides $(20 \mu\text{M})$).

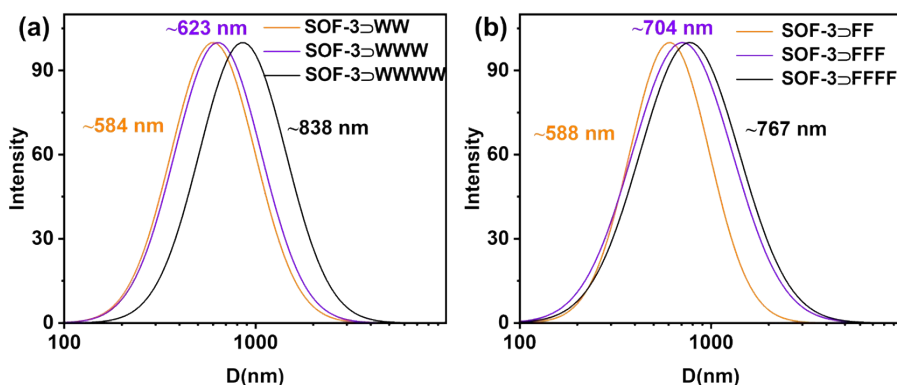


Figure S52. DLS profiles of (a) SOF-3 Δ WW (orange), SOF-3 Δ WWW (purple), SOF-3 Δ WWWW (black), and (b) SOF-3 Δ FF (orange), SOF-3 Δ FFF (purple), SOF-3 Δ FFFF (black) in water ($[3] = 10 \mu\text{M}$, $[\text{CB}[8]] = 20 \mu\text{M}$, and peptides $(20 \mu\text{M})$).

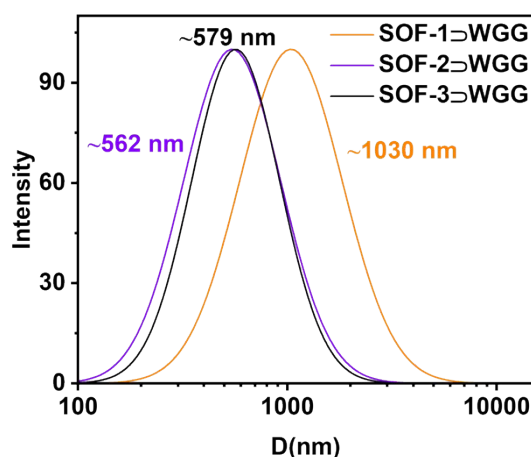


Figure S53. DLS profiles of (a) SOF-1 Δ WGG (orange), SOF-2 Δ WGG (purple), and SOF-3 Δ WGG (black) in water ($[1] = 10 \mu\text{M}$, $[2] = 10 \mu\text{M}$, $[3] = 10 \mu\text{M}$, $[\text{CB}[8]] = 20 \mu\text{M}$, and WGG $= 20 \mu\text{M}$).

Reference:

1. Li, Y.; Li, Q.; Miao, X.; Qin, C.; Chu, D.; Cao, L. Adaptive Chirality of an Achiral Cucurbit[8]uril-Based Supramolecular Organic Framework for Chirality Induction in Water, *Angew. Chem. Int. Ed.* **2021**, *60*, 6744-6751.